Ab initio simulation of the structural and electronic properties of aluminosilicate and aluminogermanate natotubes with imogolite-like structure

Fernando Alvarez-Ramírez*
Instituto Mexicano del Petróleo, Programa de Ingeniería Molecular, Eje Central Lázaro Cárdenas 152, 07730, Distrito Federal, México
(Received 2 May 2007; published 18 September 2007)

A theoretical study of imogolite-like single wall nanotubes as a function of silicon and germanium content and their tubular radius is presented along with mapping of silicon-germanium content properties in models that contain from 9 gibbsite-like units (N_u=9) to 13 gibbsite-like units (N_u=13) with a silicon-germanium content [X=Si/(Si+Ge)] of 0, 0.20, 0.40, 0.60, 0.80, and 1.00. The imogolite nanotubes were built setting periodic boundary conditions to density functional theory (DFT) geometry-optimized models along both radial and axial directions in order to obtain the stable structure. The DFT calculations were carried out on the Γ point and for various k points, using the GGA-PW91 functional, finding an optimal unit cell length of 8.72 and 8.62 Å using a double numeric (DN) and double numeric with polarization (DNP) basis set, respectively, along the axial direction. The structural properties were analyzed through the evolution of the x-ray diffraction pattern as a function of both N_u and X. A linear correlation between the tube radius and the position of the first two peaks on the x-ray diffraction is found. The imogolite surface charge was mapped with the Hirshfeld charge showing the characteristic acid tendency experimentally reported. The reactivity of imogolite-like structures was studied employing the total density of states and the band gap evolution as a function of N_u and X showing an increasing behavior with X. The local reactivity was analyzed by looking at the local density of states in models with X=0.0 and 1.0 with N_u=10. Finally, the frequency analysis was carried out in the optimized structure on the Γ point finding a good agreement in the O-H vibrations with those reported in the literature.

DOI: 10.1103/PhysRevB.76.125421 PACS number(s): 31.10.+z, 31.15.Ar, 31.15.Ew, 31.70.Ks

I. INTRODUCTION

Natural imogolite is a poor crystalline aluminosilicate with short range order whose structure consists of hollow tubes of curved gibbsite sheets, $Al(OH)_3$, with SiO_4 tetrahedra replacing hydroxy groups in the inner surface. The ideal composition is given by $(OH)_3Al_2O_3SiOH$, which manifests the atomic layer arrangement going from the exterior to the interior of the tube wall. Mineral imogolite is mostly found in soils derived from volcanic ash and in weathered pumices and spodosols.[1–5] A synthesis pathway for imogolite formation was first proposed by Farmer *et al.*[6] from diluted solutions of $Al(ClO_4)_3$ and silanol [$Si(OH)_4$]. This procedure of hydrolysis of fused sodium silicate leads to the initial formation of amorphous protoimogolite (or allophane) and the subsequent growth of crystalline imogolite tubes. Additionally, imogolites have been synthesized by tetraethoxysilane hydrolysis[7] and hydrolysis of commercial sodium silicate.[8] Wada *et al.*[9] reported the effects of substitution of a portion of silicon by germanium during the tube synthesis; they showed that the aluminogermanate tube diameter may be increased in a controlled fashion and the final synthetic 100% Ge-substituted imogolite tube contains up to 18 gibbsite units (N_u=18), based on the interaxial separation of ~30 Å.

Morphologically, imogolites show a medium to long-range order of close packed bundles of hollow fibers commonly found in association with allophane. These bundles appear as threads consisting of assemblies of tubes with thread diameters going from 10 to 30 nm.[10] The structure of imogolite bundles has been considered as a hexagonal (maximum) package configuration;[11] however, recently, x-ray powder diffraction (XRD) has shown that these bundles are better adjusted when a monoclinic unit cell is employed with the monoclinic angle (γ) equal to 78° for both aluminigermanate (100% Ge content, Imo-Ge) and aluminosilicate (100% Si content, Imo-Si) tubes.[13] Individually, each imogolite tube has an inner diameter of 0.5–0.9 nm measured by nitrogen adsorption or by transmission electron microscopy (TEM),[13–17] an outer diameter of 2.0–2.5 nm,[15,18] and lengths from several hundreds of nanometers to a micrometer. For the case of Ge-substituted imogolite, nitrogen adsorption shows a pore diameter of ~0.9 nm which is in agreement with tube dimensions.[13]

On the basis of solid state nuclear magnetic resonance (NMR), x-ray powder diffraction, and TEM, a structural imogolite atomic model was proposed[2,14,19] in which the wall of the tube consists of a curved, single sheet of gibbsite wherein the hydroxyls on one face are replaced by orthosilicate groups where the aluminum only occurs in octahedral coordination and silica in tetrahedral coordination. Electron diffraction measurements performed by Cradwick *et al.*[14] suggested that the most likely structure model of natural imogolite contains ten gibbsite units (N_u) around the circumference corresponding to a tubular diameter of 2.1±0.5 nm. On the other hand Farmer and Fraser[20] conclude that natural imogolite is composed of 12 units. The periodic distance along the tube axis was calculated from the h=0 and k=6 (hk index reflection) by Russell *et al.*[19] and Wada[2] finding a value of 8.4 Å.

From the technological point of view, imogolites are important since they show large surface areas which vary from

200 to above 700 m^2/g depending on absorbate.[17,21] Due to this surface area, together with the chemistry inherent to their surface, imogolites have been proposed as good metallic adsorbent of cations: (Cd^+, Cu^+, Pd^+),[22] (Ag^+),[23] and neutral molecules like benzene,[24] water,[25] and ammonia[26] with possible applications in the energy storage-management of methane.[27] In catalysis, imogolites have been investigated as a possible catalytic support of Cu and Pt particles.[28,29] Additionally the use of soft chemistry in the synthesis of Imo-Ge and Imo-Si allows controlling the polydispersity of both kinds of tubes that is manifested in a scarce polydispersity of the pore size distribution.[13,17] Due to its tubular structure and the existence of acid sites in the imogolite-like surface, the imogolites have been proposed as a possible shape selective catalyst with some properties similar to other aluminosilicates in a bulk phase like zeolites.[26] Furthermore, imogolites can be obtained through a direct purification of volcanic ashes; this makes the volcanic areas a reservoir with potential mineral exploitation.[26]

The aim of this paper is to report calculated structural an electronic properties and to compare them with the standard imogolite model reported by Wada *et al.*[2,9] and by Farmer *et al.*[3] as a function of silicon-germanium content and gibbsite units. In order to test the structural mesoscale arrangement of imogolite bundles, the experimental results from x-ray diffraction have been selected since this technique is one of the most used to structurally characterize imogolite-like structures.[13,27,30,31] We compare the experimental x-ray results with those generated by our density functional theory (DFT) for our geometry optimized periodic models and correlate experimental and theoretical results. Finally, in order to elucidate some aspects of the infrared (IR) and Raman spectra of imogolite, the experimental IR spectra is compared with the frequency analysis of the optimized $N_u=10$ structure on the Γ point approximation, due to the high level computational cost of this kind of calculations.

The theoretical work on atomistic models of imogolite can be divided into two main approaches, the force field and *ab initio* methodologies, for the description of atomic interactions. In the first approach the interatomic potential between atoms is described through force fields that allow treating systems with a large number of atoms as is the case of imogolite structure. The force field methodology has been used by Tamura *et al.*[11] developing a three-body parametrized potential and reporting the strain energy, pair distribution functions, and vibrational spectra of imogolite models. Additionally, Konduri *et al.*[12] has recently used the CLAYFF force field to determine the strain energies and the vibrational spectra in atomistic imogolite models. The *ab initio* theoretical calculations have not been attempted, due mainly to the size of the unit cell, recently Abidin *et al.*[32] carried out molecular orbital calculations of orthosilicate, gibbsite, and protoimogolite models showing that the dissociation of the Si-OH plays an important role in the formation of allophone and imogolite, but we have calculated electronic properties [band structure, electronic density of states (DOS), electrostatic potential, atomic electrostatic charges] and DFT geometry optimized structures for complete imogolite-like tubes using *ab initio* methods. The main limitation in these types of calculations is the size of the models

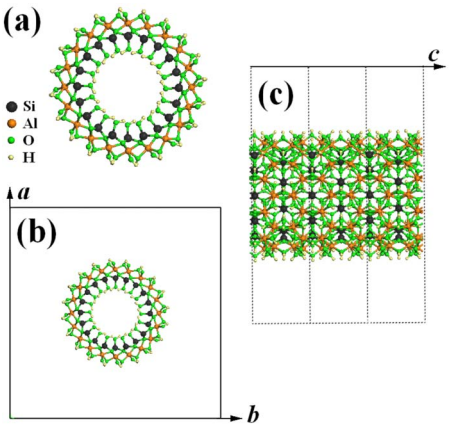

FIG. 1. (Color online) (a) Cross sectional view of an imogolite structure with ten gibbsite units. (b) The imogolite model is inserted in a periodic boundary cell with cell dimensions $a=40$ Å and $b=40$ Å in order to avoid interactions with periodic images. (c) Periodic boundary condition along the c direction in the simulation cell.

and consequently a coarser k-point grid description has to be used compared with more tractable systems sizes; however, useful qualitative results can be obtained for properties like surface acidity, and adsorption of molecules and ions by these idealized nonhydrated tubes.

II. STRUCTURAL GENERATION OF MODELS

Imogolite-like structures are constituted by a curved gibbsite cylinder with tetrahedral Si-OH replacing hydroxy groups in the inner surface of the gibbsite layer. A standard model for the construction of the cylindrical unit cell atomic arrangement was proposed by Cradwick *et al.*[14] using symmetry properties for the generation of even and odd numbers of gibbsite units in the cylindrical unit cell. In our case, we have followed a different path; we make a direct transformation of a gibbsite monolayer, with the hydroxyl groups on one side substituted by Si-OH; then we apply a linear transformation of coordinates from the flat arrangement to the cylindrical configuration. In this process we keep the gibbsite length b constant (8.4 Å), which corresponds to the period along the tube axis c. Using this cylindrical structure, periodic three-dimensional models were constructed with unit cell dimensions $a=b=40$ Å, in order to avoid possible interactions between the different imogolite images on the periodic model, and the c dimension of the unit cell (period of the cylindrical structure) equal to 8.4 Å, see Fig. 1. However, along the c direction there are small variations in the reported values that go from 8.4 Å[2,14,19] to 8.5 Å;[13] also Wada *et al.*[7] have reported a $2\theta=12°$ x-ray peak at a value of 8.74 Å, possibly due to the scattering of individual tubes that may be ascribed to a c value; because of these small variations of c we carried out a sequence of geometry optimization processes on two models: Imo-Si and Imo-Ge, with $N_u=10$ gibbsite units, that corresponds to the most likely structure of natural imogolite.

The energy *vs* c length mapping for $N_u=10$ Imo-Si and

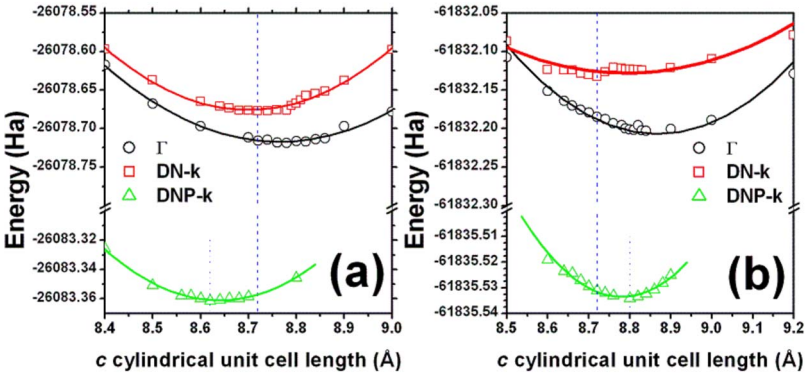

FIG. 2. (Color online) Energy values as a function of the cylindrical cell length *c* for the cases of Imo-Si (a) and Imo-Ge (b). The square symbols are the geometry optimized energies of Imo-Si and Imo-Ge for the Γ point approximation; the open circles are the energies for the various *k* points calculations for both types of tubes, triangles are the energies for the various *k* points calculations using a DNP basis set. The dotted lines show the minimum position for the various *k* points calculation localized in 8.72 Å for both cases (a) and (b), using a DN basis set, and 8.62 Å (a) and 8.8 Å (b) with the DNP basis.

Imo-Ge is presented in Fig. 2. The relaxation of structural models was performed keeping *a* and *b* cell dimensions constant and mapping the *ab initio* relaxed structure energy as a function of *c* cell length. In these sequences of geometry optimization calculations we use the DFT code DMol3[33–35] with the GGA Perdew-Wang 91 functional (PW91)[36] and the double numeric (DN) and double numeric with polarization (DNP) numerical basis set. On the reciprocal space two kinds of calculations were carried out, for the first one only the Γ point was considered, which could be a good approximation based on the fact that the size of the cylindrical unit cell in our models is large enough and the reciprocal space cell size is inversely proportional to the size of the cell dimensions. However, the consideration of the Γ point alone could not take into account the long range interactions in the pseudocrystalline structure along the *c* axis. For this reason a second sequence of calculations, considering various *k* points, was performed, see Table I.

As can be seen in Fig. 2, a minimum potential well is found at 8.78 Å for the case of Imo-Si and 8.8 Å for the case of Imo-Ge considering only the Γ point and a DN basis set. For the case of the calculation for various *k* points and a DN basis set, we found the minimum potential well position in both Imo-Si and Imo-Ge at 8.72 Å. These values differ in about 0.2 to 0.3 Å with respect to the established values of 8.4 to 8.5 Å reported in literature, but closer to the reported value of 8.74 Å quoted by Wada *et al.*[7] possibly due to the scattering of individual tubes; in addition it is noted that the various *k* points calculations differ by 0.02 Å from the Wada result along the *c* cylindrical cell length. In order to discern if these variations in the cylindrical unit cell are produced by the basis set selected in the geometry optimization of the imogolite structures, a new potential well was calculated with the same DFT parameters used in the DN basis-various *k* points calculations, but changing the basis set from DN to DNP which is a bigger basis set. The use of the DNP basis set changes the minimum position of the Imo-Si *c* cylindrical unit cell length to 8.62 Å that is closer to the experimental values of 8.4 to 8.5 Å than the DN basis set but it is still bigger, see Fig. 2(a). In the case of Imo-Ge the DNP calculation with various *k* points produces a larger *c* cylindrical unit cell length minimum position than the DN basis set, having the minimum at 8.8 Å, see Fig. 2(b).

TABLE I. *k* vectors used in the geometry optimization of tubular imogolites.

Symbol		*k*-vector		Weight
K1	0.00000	0.42857	0.00000	0.285714
K2	0.00000	0.28571	0.00000	0.285714
K3	0.00000	0.14286	0.00000	0.285714
Γ	0.00000	0.00000	0.00000	0.142857

The variations on the theoretical values of the *c* cylindrical unit cell could have their origin in curvature effects of the imogolite layer; therefore in order to elucidate if the values of the *c* cylindrical unit cell length (the *b* length of the gibbsite cell) are due to the curvature of the imogolite tubular structure, a mapping of geometry optimized structures as a function of the cell lengths *a* and *b* for a layered imogolite-like structure was carried out, see Fig. 3(a). The DFT DMol3 geometry optimization parameters used in these calculations are the same as those used in the tubular structure optimizations using a DNP basis set, but now taking more *k* points than for the tubular case, since the basic cell is now smaller and more manageable from the computational point of view, see Table II. The results of these optimizations show the lower values for the energy for lengths *a* and *b* in 4.9 and 8.46 Å, respectively, Figs. 3(b) and 3(c). The values of the *b* cell length at 8.46 Å is in the experimental interval reported for tubular imogolite 8.4 to 8.5 Å, meanwhile the *a* cell length is in the interval of the corresponding gibbsite length.

From this analysis, we can conclude that the *b* dimension of the cell for the flat imogolite-like structure is of the same order of magnitude than in the gibbsite structure; the variation of the *c* cylindrical unit cell length could be due to two factors: the first is that *c* may have a dependence on the curvature of the imogolite layer, however, if this were the case the variation is so small (approximately 0.2 Å in a cell of 8.5 Å) that the deviations in the nearest-neighbors interatomic lengths would be of the same order of magnitude and can be neglected. The second factor could be attributed to the calculation itself since it may be necessary to increase the basis set and the number of *k* points considered in order to reach the experimental values of *c*; if this were the case, the increment of the *k* points and the basis set would improve significantly the electronic properties obtained with lower basis set and *k* points. However, the electronic properties of the system calculated at four different theory levels: (1) tubular imogolite calculated with a basis set DN and in the Γ point (Imo-Si-Γ-DN), (2) tubular imogolite calculated with a

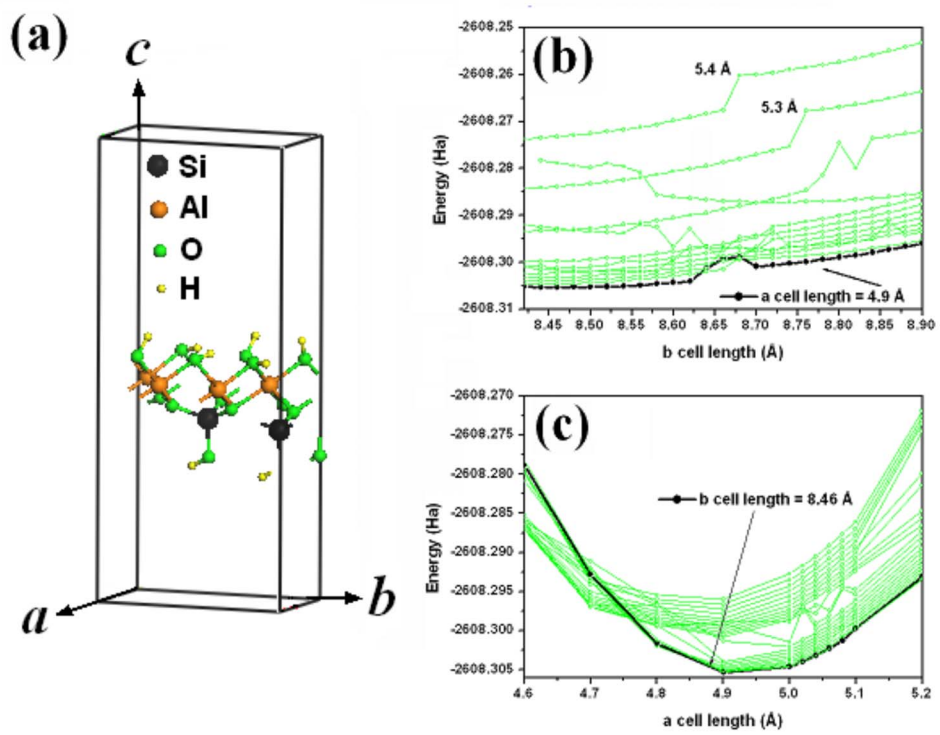

FIG. 3. (Color online) (a) Basic cell of flat imogolite, corresponding to the case where the tube has an infinite radius. (b) Energy curves of the geometry optimized cell for the flat imogolite as a function of b cell length, the lines are only as a guide for the eye and indicate a constant value of the a cell length. The minimum value was found in b=8.46 Å. (c) Energy curves of the geometry optimized cell for the flat imogolite as a function of a, the minimum value was found for a=4.9 Å.

basis set DN and with various k points (Imo-Si-k-DN), (3) tubular imogolite calculated with a basis set DNP and with various k points (Imo-Si-k-DNP), and (4) flat imogolite with various k points and the DNP basis set, generate the same behavior on the Hirshfeld charge distribution as a function of the tube radius, in the case of tubular structures, and as a function of the z position, in the case of flat imogolite, see Fig. 4. The DN basis set produces a somewhat larger value of the Hirshfeld charges than the calculations with DNP and seems to be independent of the k points set selected, see Figs. 4(a) and 4(b). For the DNP basis set calculations, the charge analysis shows very small changes between the tubular structure and the flat one, both calculated with various k points. Therefore it can be seen that in a qualitative way the charge distribution analysis of imogolite structures is essentially independent of the basis set and of the number of k points selected.

The density of states (DOS) of the four systems shows the same qualitative behavior and the same morphology. In all cases the DOS display an empty band gap value of 4.752 eV for the case of DN-Γ, 4.786 eV in the case of DN-k, 4.940 eV in the case of DNP-k, and 5.574 eV for the flat

TABLE II. k vectors used in the geometry optimization for the flat imogolite structure.

		k-vector		Weight
0.3333	0.00000	0.42857	0.00000	0.285714
0.3333	0.00000	0.28571	0.00000	0.285714
0.3333	0.00000	0.14286	0.00000	0.285714
0.3333	0.00000	0.00000	0.00000	0.142857
0.3333	0.3333	0.3333	0.3333	0.3333

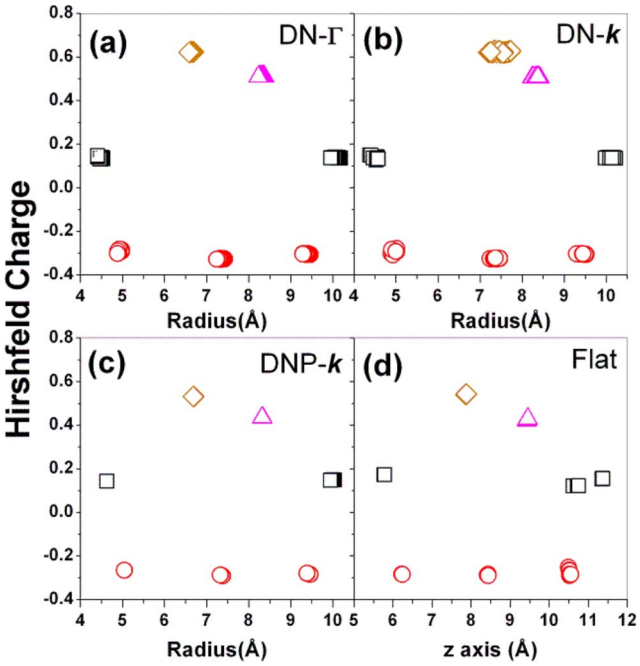

FIG. 4. (Color online) Hirshfeld charge analysis as function of the radius of the geometry optimized tubular Imo-Si structures calculated with (a) DN basis set and Γ, (b) DN basis set and various k points (Table I), and (c) DNP basis set and various k points (Table I). Hirshfeld charge analysis as a function of z position in (d) flat imogolite calculated with a DNP basis set and various k points (Table II). In all cases the qualitative behavior is the same which makes the Hirshfeld analysis independent of the basis set and of the k points selected. The notation indicates hydrogen □, oxygen ○, silicon ◇, aluminum △, and germanium ⋆.

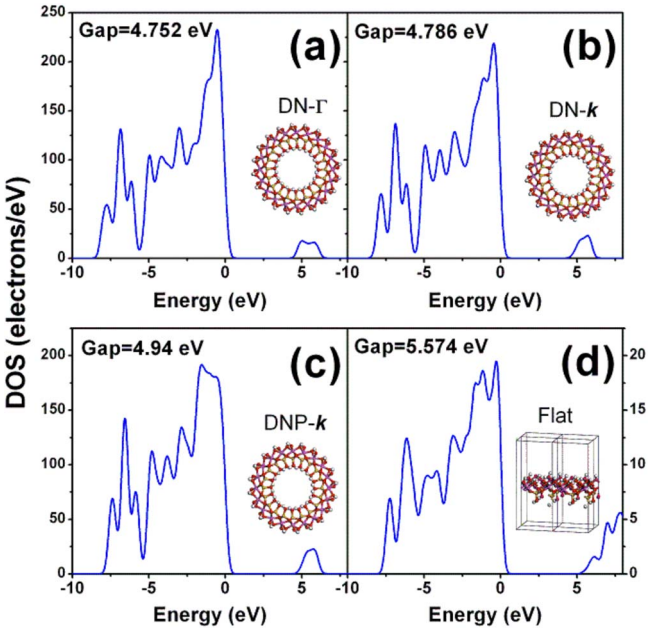

FIG. 5. (Color online) DOS for tubular imogolite structures (Imo-Si) calculated with (a) DN basis set and at $\Gamma(0,0,0)$, in the reciprocal space. (b) DN basis set and various k points (Table I), and (c) DNP basis set and various k points (Table I). DOS for (d) the flat imogolite calculated with DNP basis set and various k points (Table II).

imogolite. In all cases, the morphology of the DOS curves shows the same qualitative behavior, see Fig. 5. This seems to indicate that the qualitative electronic behavior of the imogolite-like structures is independent of the basis set and of the number of k points in the case of tubular structures, and shows a larger band gap for the case of flat imogolite (infinite radius tube).

Since the variations of the c cell values for Imo-Ge and Imo-Si are small compared with the cell length ($\sim 2\%$), and due to the fact that the qualitative properties of imogolite structures derived from the studied theory level (DN-Γ, DN-k, and DNP-k) are the same, in what follows the DN basis set will be chosen as a reasonable approximation to the electronic properties, thereby optimizing the computational resources. Due to the fact that the DN basis set generates practically the same c length for Imo-Si and Imo-Ge, we assume that the c length is the same for all other $X=\mathrm{Si}/(\mathrm{Si}+\mathrm{Ge})$ values. Furthermore, we also assume that the c length is independent of the number of gibbsite units N_u in the tube structure. Therefore in this work a c value of 8.8 Å for the DN-Γ approximation and of 8.72 Å for the DN-k calculation is going to be assumed throughout.

The x-ray technique has been extensively used by experimental groups in the characterization of both isolated and bundles of imogolite-like tubes and their structural evolution during their synthesis,[13,27,30,31,37,38] the results obtained using this technique depend on whether the imogolite-like samples are isolated tubes or bundles. The isolated tubes are obtained by dispersion with ultrasonification in an ice bath[38] from a common bundle arrangement. However, as far as we know, there is nosystematic theoretical study of the x-ray diffraction evolution as a function of both silicon and germanium content and the number N_u of gibbsite units in the tube. Therefore we have studied the evolution of the x-ray diffraction pattern (x-ray-P) for both isolated imogolite-like tubes and bundles. For the case of isolated imogolite x-ray-P, the a and b values of the cylindrical unit cell were increased to 100 Å in order to avoid possible interference diffractions along these directions, see Fig. 1(b). The x-ray-P was obtained using the Cerius2 diffraction-crystal module[39] with two different x-ray sources ($K\alpha$-Cu and $K\alpha$-Fe) and a polarization fraction of 0.5 assuming the system is in powder form. The results of x-Ray-P are shown in Fig. 6 as a function of the silicon content, $X=\mathrm{Si}/(\mathrm{Si}+\mathrm{Ge})$, the number of gibbsite units, and for both x-ray sources, iron and copper. The x-ray-P are scarcely sensitive to X content and show practically no differences in the region between $2\theta=20°$ and 30°, for both sources; the differences are observed mainly in the region $2\theta<20°$ where the two main observed peaks evolve as a function of N_u. These two peaks are shifted toward lower 2θ values for bigger tube radii, and their 2θ peak center evolution follows a linear relation as a function of N_u, see Table III. This feature allows identifying the N_u in the tubular structures directly from the x-ray-P.

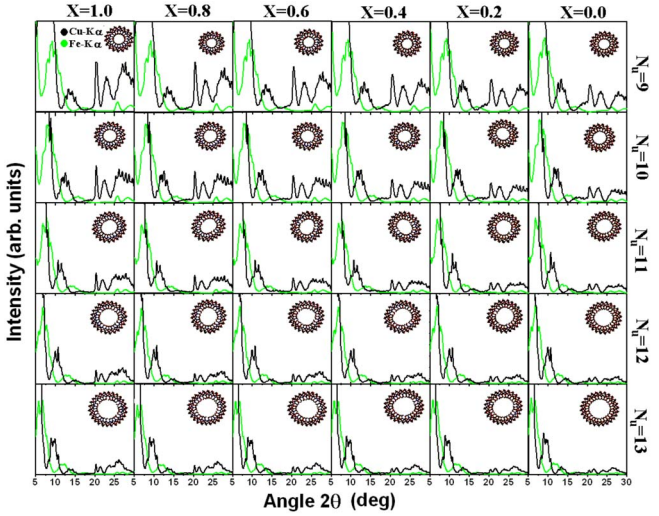

FIG. 6. (Color online) X-ray diffraction pattern (x-ray-P) of imogolite-like structures as a function of N_u, and the Si content, $\mathrm{Si}/(\mathrm{Si}+\mathrm{Ge})$. The red line is the simulated x-ray-P using $K\alpha$-Fe as a source and the blue line is the x-ray-P using $K\alpha$-Cu as a source.

TABLE III. Linear fit parameters for the x-ray-P peaks in the region $8° < 2\theta < 20°$. The parameters correspond to the linear equation $2\theta_{xy}=\mathbf{m}N_u+\mathbf{b}$, where x indicates the first or the second peak, y indicates the source in the x-ray-P calculation, and N_u the number of gibbsite units in the tubular structure.

2θ	**m**	**b**
$2\theta_{1\mathrm{Fe}}$	−0.75925	16.00133
$2\theta_{2\mathrm{Fe}}$	−1.35917	29.42073
$2\theta_{1\mathrm{Cu}}$	−1.06764	23.18161
$2\theta_{2\mathrm{Cu}}$	−1.51764	33.43214

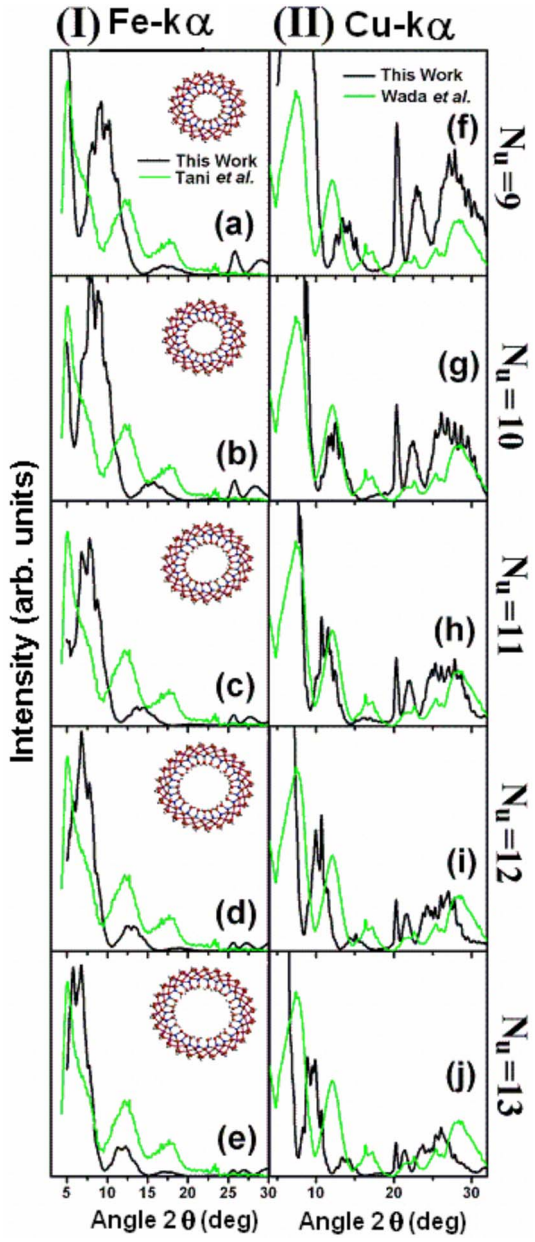

FIG. 7. (Color online) (I) (a)–(e) Comparison of experimental x-ray-P obtained by Tani *et al.* (Ref. 38) using $K\alpha$-Fe as the x-ray source with the simulated x-ray-P for the same source in the interval $9 \leq N_u \leq 13$, the best agreement occurs for (e) with $N_u=13$. (II) (f)–(j) Comparison of experimental x-ray-P obtained by Wada *et al.* (Ref. 9) using $K\alpha$-Cu as the x-ray source with simulated x-ray-P for $9 \leq N_u \leq 13$, the best agreement is found for both $N_u=10$ (g) and $N_u=11$ (h).

In Fig. 7, the theoretical x-ray-P are compared with two experimental x-ray-P for the case of Imo-Si. The sequence of patterns (I) shows the comparison of the experimental x-ray-P obtained by Tani *et al.*[38] for synthetic 100% Si imogolite and $K\alpha$-Fe with the x-ray-P calculated in this work for the same source. In this sequence a shift of the two main calculated peaks in the region $5° < 2\theta < 30°$ can be observed, and a third peak starts to appear at $N_u=11$ in the region $15° < 2\theta < 20°$ and it is well-defined at $N_u=13$. The best agreement between the experimental curve obtained by Tani *et al.* and our simulated results is found for $N_u=13$, Fig. 7(e). Another theoretical and experimental comparison is presented in sequence (II) where the experimental x-ray-P was obtained by Wada *et al.*[9] for natural imogolite with $K\alpha$-Cu. A shift toward lower 2θ with increasing N_u is observed and the best agreement between theory and experiment occurs for both $N_u=10$ and 11. This result is in accordance with what has been accepted as the most likely value of $N_u=10$ for natural imogolite.[14,40]

In the mesoscale level, imogolites are characterized by bundles containing 3–20 tubes essentially randomly oriented;[9,13,15,22,30,31,38,41–43] in some cases local ordering appears in the tube orientation.[17] The mesoscale structural properties of oriented tubes have been simulated by Hoshino *et al.*[44] assembling the cylindrical tubes aligned in a packed hexagonal structure, testing different bundle configurations and comparing the simulated pair distribution functions with experimental ones obtained by small angle x-ray scattering. There is a controversy between the hexagonal intertubular package configuration used by Tamura *et al.*[11] in their molecular dynamics simulations and also used by Pohl *et al.*[40] in their structural models *versus* the monoclinic arrangement suggested by Mukherjee *et al.* on the basis of x-ray diffraction spectra of synthetic thin films of both Imo-Si and Imo-Ge. Mukherjee *et al.* proposed a cylindrical cell with dimensions $a=b=2.105$ nm, $c=0.851$ nm; $\alpha=\beta=90°$ and $\gamma=78°$, and $a=b=3.253$ nm, $c=0.851$ nm; $\alpha=\beta=90°$ and $\gamma=78°$ for Imo-Si and Imo-Ge, respectively.

In order to discern between the hexagonal and the monoclinic arrangements a sequence of calculations for the two corresponding γ angles, the intertubular distance, and N_u were carried out. These simulations were performed using periodic boundary conditions of 5×5 Imo-Si arrangements with the intertubular distances $a=b$ varying from 2.0 to 5.0 nm, and N_u varying from 10 to 14. In all cases the axial cell distance c was kept fixed and equal to 8.72 Å. The interbundle distances $A=B$ were also kept fixed and equal to 40 nm to elucidate only the effects of the γ angle in a single bundle configuration, see Fig. 8(a). The computational parameters used in the imogolite bundle x-ray-P simulations are exactly the same as for the single isolated tube x-ray-P simulations. The results for the imogolite bundle were compared with the experimental work of Mukherjee *et al.*[13] for Imo-Si in both hexagonal and monoclinic arrangements. The comparison of the simulated and experimental x-ray-P for the case of a hexagonal arrangement, $\gamma=60°$, as a function of the gibbsite units, N_u, and the intertubular distance (ITD) are shown in Fig. 9; the best agreement for the lower region, distances smaller than 12 Å, occurs for the case of $N_u=12$. This fact ratifies the results found in the isolated tube simulation of the x-ray-P pattern where it is shown that the two first peaks in the lower region identify the average tube diameter. The simulated x-ray-P shows large fluctuations for distances larger that 12 Å when the ITD is changed, but from the sequence of theoretical and experimental comparisons, shown in Fig. 9, we can observe that the best agreement for a hexagonal arrangement is found when $N_u=12$ and ITD $=26$ Å.

A comparison between the experimental x-ray-P obtained

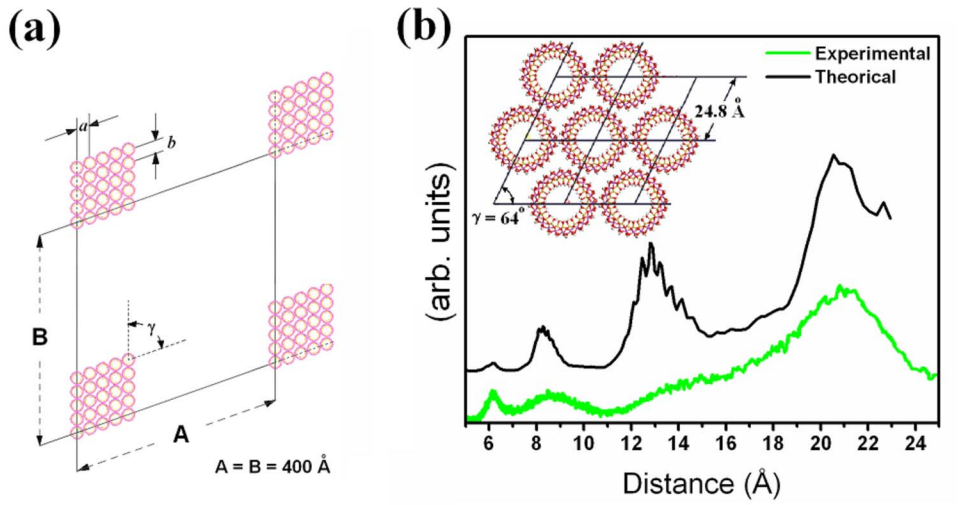

FIG. 8. (Color online) (a) Periodic boundary conditions used in the mesoscale x-Ray-P simulation. The cell lengths A and B were fixed to 400 Å. It was varied both the angle θ from 60° to 90° in intervals of 2° and the separation between individual tubes varying the a and b distances in the same amount. (c) Comparison between experimental x-Ray-P of synthetic imogolite obtained by Mukherjee *et al.*[13] and simulated x-Ray-P with a bunch of tubes with $N_u=12$, $a=b=24.8$ Å, and $\theta=64°$.

by Mukherjee *et al.*[13] and the simulated x-ray-P of imogolite tubes in a monoclinic arrangement with $\gamma=80°$, as a function of the gibbsite units, N_u, and the intertubular distance ITD is shown in Fig. 10. The simulated x-ray-P shows large fluctuations in the position peaks when the tube size and the intertubular distance are changed. However, as in the case of a hexagonal arrangement the best agreement in the lower region is found when $N_u=12$, thereby determining the radius of the tube. On the other hand, the x-ray-P for distances larger than 12 Å is very sensitive to the tube arrangement, finding the best agreement in the case of ITD=28 and 30 Å. The simulated monoclinic case with $\gamma=80°$ is close to the experimental value given by Mukherjee *et al.* with $\gamma=78°$, therefore our calculations can be considered as a good approximation to the experimental results. A close analysis in the ITD, gibbsite units N_u, and the γ angle in the bundle tubular arrangement indicates that from our point of view, the best agreement between experiment and simulation is found for $N_u=12$, $a=b=2.48$ nm, and $\gamma=64°$, Fig. 8(b). The positions of the two peaks located between 5 and 10 Å can be explained using $N_u=12$ whereas the position of the peaks at 13 and 21 Å can be explained in a simple minded way as due to small variations from the hexagonal arrangement. However, it should be considered that our simulation is just a *simplification* of the real case where the instrumental broadening parameters, and preferred orientation of the bundles, should be considered in order to give a definitive answer about the intertubular arrangement in the imogolite bundles. Nevertheless, these simplified simulations shed light on some aspects of the x-ray-P of imogolite tubes at the mesoscopic level.

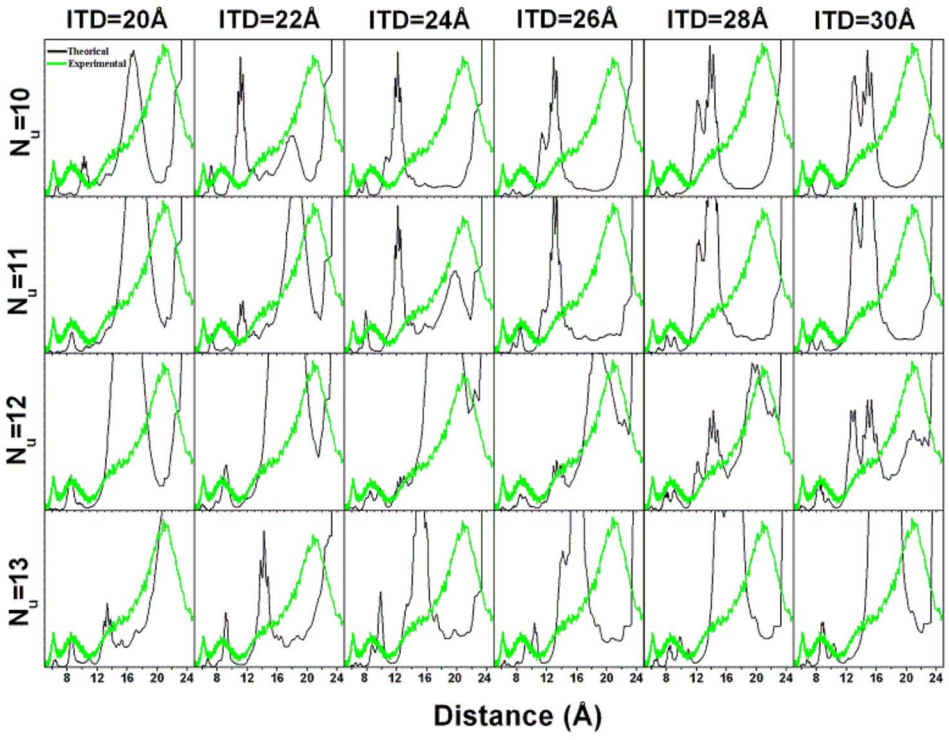

FIG. 9. (Color online) Sequence of simulated x-ray-P for the hexagonal macroscopic arrangement, $\gamma=60°$, of the imogolite tubes as function of the gibbsite units N_u and the intertubular distance (ITD). In all the cases the simulated x-ray-P is compared with the experimental curve reported by Mukherjee *et al.* (Ref. 13) finding the best agreement when $N_u=12$ and ITD=26 Å.

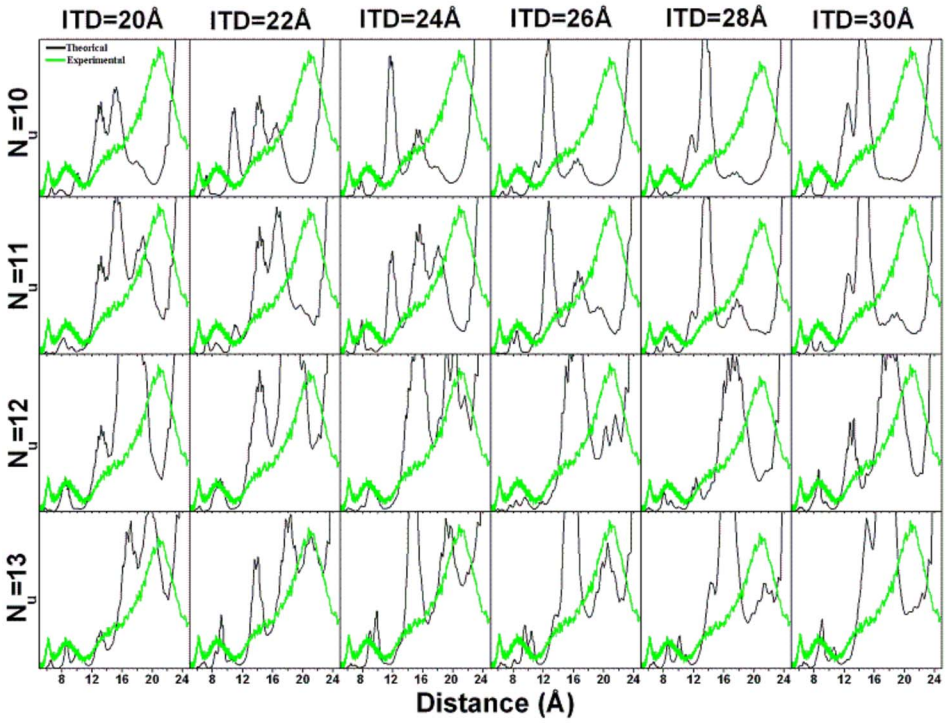

FIG. 10. (Color online) Sequence of simulated x-Ray-P for monoclinic mesoscopic arrangement, $\gamma=80°$, of the imogolite bundle as a function of the gibbsite units N_u and the ITD. In all the cases the simulated x-Ray-P is compared with the experimental curve reported by Mukherjee *et al.* (Ref. 13); the best agreement occurs for the case $N_u=12$, and both ITD=28 and ITD=30 Å.

III. ELECTRONIC PROPERTIES

The imogolite electronic properties and, especially, the imogolite surface electronic properties are a determining factor on the sorption properties and reactivity of these minerals. Imogolites have adsorption properties of cations (Cd^+, Cu^+, Pd^+)[22] and (Ag^+),[23] neutral molecules like benzene,[24] water,[25] ammonia,[26] and possible applications in the energy storage-management of methane.[27] Additionally, the adsoption of chlorite by imogolites in a wide *p*H range[45] is well-known, and it has been suggested the existence of a high point of zero charge in the outer parts of the imogolite, based on electrophoretic mobility studies.[46] The sorption of this variety of ions and molecules is linked to the electronic charge distribution on the imogolite tube, which depends on the curvature of the tube. Gustafsson[47] argues that the deformation of Al-O bonds can explain a weak positive charge on the outer walls and a weak negative charge on the inner walls of imogolite.

Because of the importance of spatial charge distribution and the effects of the curvature in the charge values, we have examined the atomic electrostatic charges in all the geometry optimized imogolite-like structures computed from the *ab initio* calculations as a function of both N_u and content X. The Hirshfeld charge population analysis was selected to determine the surface charges which were plotted as a function of tube radius, taking the cylindrical cell center as the center of tube structure, see Fig. 11. For clarity in the charge analysis, an annotation to the radial sequence of atoms from the inner to the outer layers was attached; therefore H_1 indicates the hydrogen in the inner radial imogolite atomic array, O_2 is the oxygen in the second layer, and Si_3 (or Ge_3), O_4, Al_5, O_6, and H_7 for the rest of the arrangement. The sequence of charge distribution shows small atomic charge fluctuations between atoms of the same element and relative radial position in the tube atomic array, independently of the tube curvature, Fig. 11. The inner and outer layers H_1 and H_7 show essentially the same positive charge values $\sim$0.13 that are independent of tube radius and composition. Geometrically, H_1 is the limit of the inner pore, whose size has been measured to be between 0.5 and 0.9 nm[13–17] and H_7 is the outer limit diameter of the tube, 2.0–2.5 nm.[15,18] From Fig. 11 it can be seen that the calculated inner and outer radii of our structures is within the range of the experimentally reported values, the average values are reported in Table IV.

A similar behavior in the radial charge distribution is observed for Imo-Ge therefore it can be concluded that the substitution of silicon by germanium in the imogolite structure does not modify significantly the radial positions. The radial position fluctuation of non pure systems $X=0.2$, 0.4, 0.6, and 0.8 are larger than the pure systems Imo-Si and Imo-Ge, due to the deviations of the cylindrical geometry in these contents generated by the small change in the atomic size of germanium compared with silicon, see Fig. 6 and 11. The Hirshfeld charge for oxygen can be classified in two groups: the first group contains O_2 and O_6 and the second group contains only O_4; the second group shows a bigger negative charge than the first group, with average values of -0.273, -0.324, and -0.305 for O_2, O_4, and O_6, respectively. The Al_5 charge values are very stable in all the configurations produced by the high symmetry octahedral structure with an atomic charge average value of 0.506. Similar average charge behavior is shown by Si_3 and Ge_3 with Ge_3 having a bigger charge than Si_3, 0.670 versus 0.616. The local distribution of atomic charges generates a positive charge in both, inner and outer faces of imogolites, despite the neutrality of the systems.

Imogolite has been proposed as a possible shape selective catalyst material[26,28] and as a catalytic support for particles

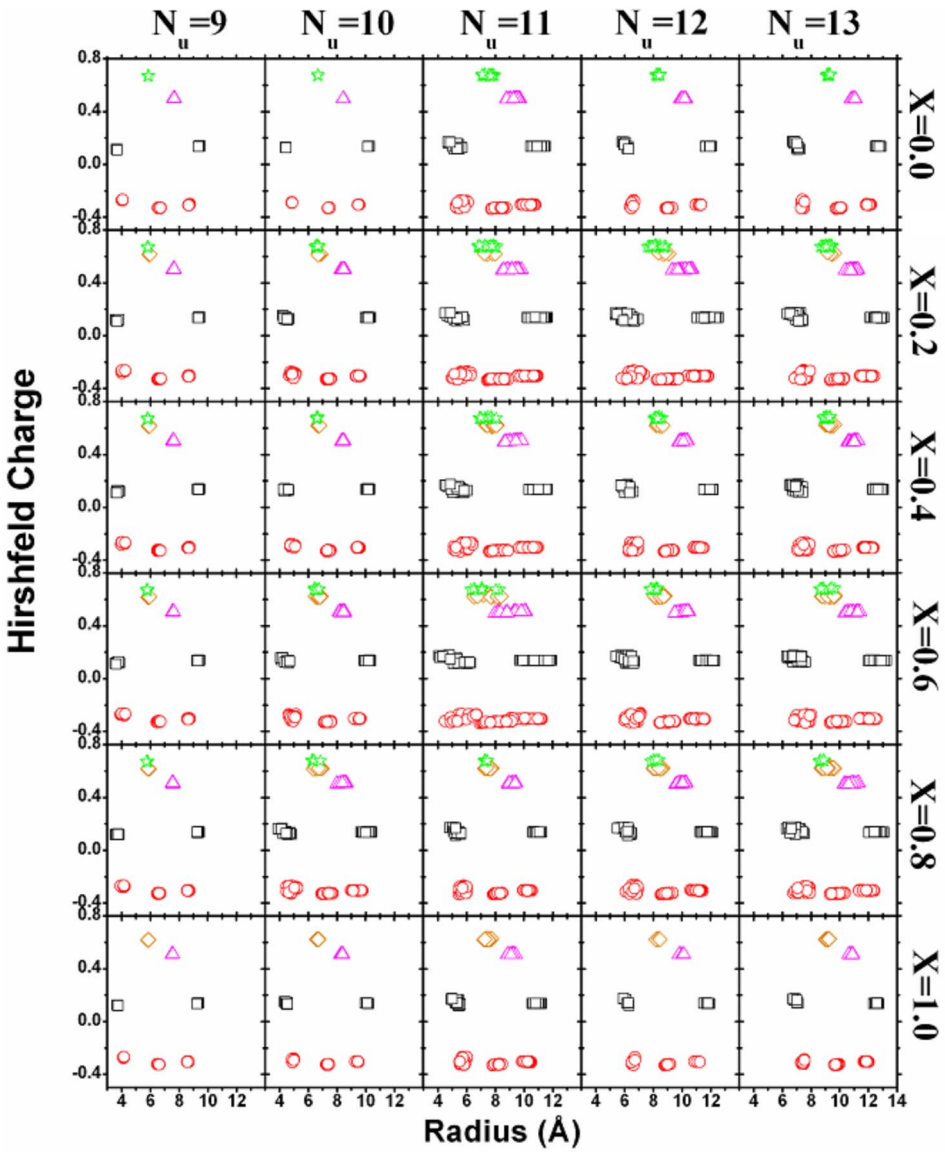

FIG. 11. (Color online) Hirshfeld charge analysis as function of the number of gibbsite units N_u in the tube, of the silicon content X, and of the position along the tube radius. The notation indicates hydrogen □, oxygen ○, silicon ◇, aluminum △, and germanium ⋆. The fluctuations in $N_u=11$ and $X=0.6$ are produced by distortions from the perfect cylindrical shape in the optimized geometry.

of Cu and Pt (Refs. 28 and 29) with surface areas of 1000 m^2/g measured by ethylene glycol[48] and ~300–400 m^2/g measured by N_2 adsoption.[17] Imogolite shows reactive properties towards anions and cations[6] but the mechanism of this reactivity is not well-known. The origin of the affinity of imogolite to the sorption anions and cations could have its origin not only in electrostatic interaction but also in purely chemical interactions with imogolite surfaces; for the latter case it would be necessary to understand the electronic configuration of the imogolite structure as a first step.

TABLE IV. Evolution of the average inner and outer radial position of H_1 and H_7 as a function of the number of gibbsite units in Imo-Si.

$2N_u$	r_{inner} (Å)	r_{outer} (Å)
9	3.75	9.32
10	4.51	10.12
11	5.33	10.93
12	6.14	11.74
12	6.94	12.56

In order to have a better understanding of the correlation between the electronic states within the DOS and the geometric radial position, the local density of states (LDOS) was calculated for Imo-Si and Imo-Ge with $N_u=10$ using the CASTEP[49] code with the GGA Perdew-Wang 91 functional (PW91); the cutoff in the plane waves expansion was chosen as 10 eV and the calculations were carried out for the Γ point. In Fig. 12 the composition of DOS in terms of LDOS is shown and it can be seen that for the case of Imo-Si the contributions of H_1, Si_3, Al_5, and H_7 to the density of states in the neighborhood of the highest occupied molecular orbital (HOMO) energy is nonexistent, see Fig. 12(a); the main contribution to this region comes from the oxygen layers. The oxygen electronic states coming from the layer O_2 has a lower contribution than the other two oxygen layers O_4 and

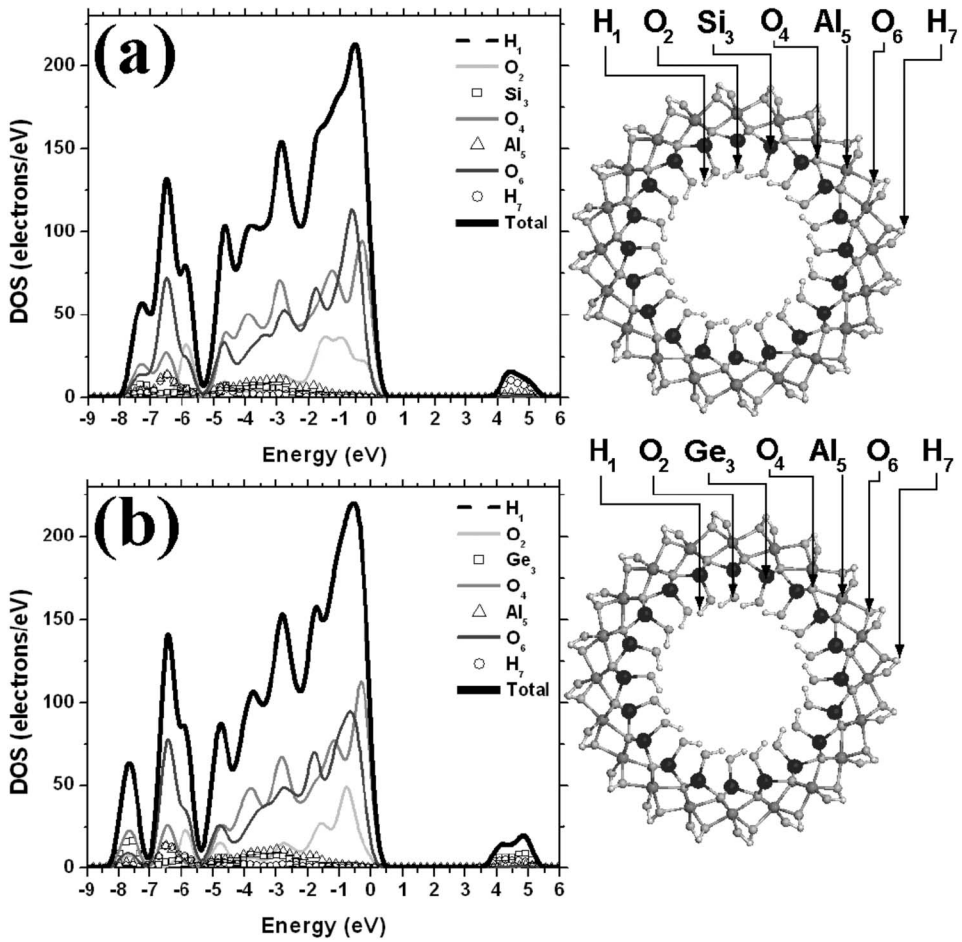

FIG. 12. Radial local density of states analysis of $N_u=10$ Imo-Si in (a) and Imo-Ge in (b). The contributions in the HOMO region come from oxygen positions and in particular from the O_4 atomic radial layer in both cases. In the conduction band the main contributions come from H_7 for Imo-Si and both H_7 and Ge_3 for Imo-Ge.

O_6; in particular O_6 has the largest peak contribution to the total DOS but its position in the energy axis is shifted towards lower values. The O_4 oxygen layer is the major contributor to the HOMO region; the conduction band is formed mainly by the states from the H_7 layer. Similar behavior is observed for the case of Imo-Ge: the states with energies near HOMO come from oxygen layers O_2, O_4, and O_6, whereas the contribution of the layers H_1, Ge_3, Al_5, and H_7 is scarce. For the case of Imo-Ge the contribution of oxygen layers follows a similar behavior to the Imo-Si case in the energy axis, but there is an increment on the density of states coming from the O_4 layer produced by the introduction of germanium in its vicinity, Fig. 12(b). Furthermore, the conduction band shows two main contributions, the first one coming from the H_7 layer as for Imo-Si, and the second one, the largest, coming from the germanium layer. On the basis of this LDOS study if one electron is extracted from the imogolite structure forming the cation-imogolite (Imo-Si^+, Imo-Ge^+) the states most affected are those that come from the oxygen layers and in particular the internal O_4 layer, independent of the composition X, meanwhile in anion imogolite (Imo-Si^-, Imo-Ge^-) the states most affected are those coming from the H_7 layer electronic states for both cases; in the case of Imo-Ge^-, the Ge_3 layer electronic states are also altered.

The chemical reactivity of imogolite-like structures can be analyzed by the electronic band gap as a function of the composition X. The imogolite-like structures show a tendency that the larger the concentration of Ge the smaller the band gap, see Figs. 13(a)–13(d). This behavior is independent of the different tubular radial dimensions N_u when the four k points are considered, showing the same general increasing tendency with fluctuations of at most 0.2 eV. Therefore the electronic softness and hardness of imogolite fibers are functions of the Ge content X as a consequence of the behavior of the band gap. The imogolite variable band gap values of 4.3–4.8 eV at the Γ point makes the imogolite structures an insulator; however, these results must be limited to the ideal nonhydrated imogolites systems and they must be considered just a first approximation to the real hydrated problem, where the surface electronic structure will change substantially with pH and hydration.

IV. FREQUENCY ANALYSIS ON IMO-SI, $N_u=10$

The IR and Raman spectra, both associated to the normal modes of vibration, are two of the most used techniques of characterization of imogolite fibers.[9,22,29–31,38,41,42,50] The interpretation of the IR and Raman spectra is a complicated issue, especially in systems with many degrees of freedom like in large molecules or fibers where it is possible to find vibrations associated to some atomic groups, but also some collective modes (phonons) due to the large size of the fibers. Experimentally, the imogolite IR spectra exhibit some typical

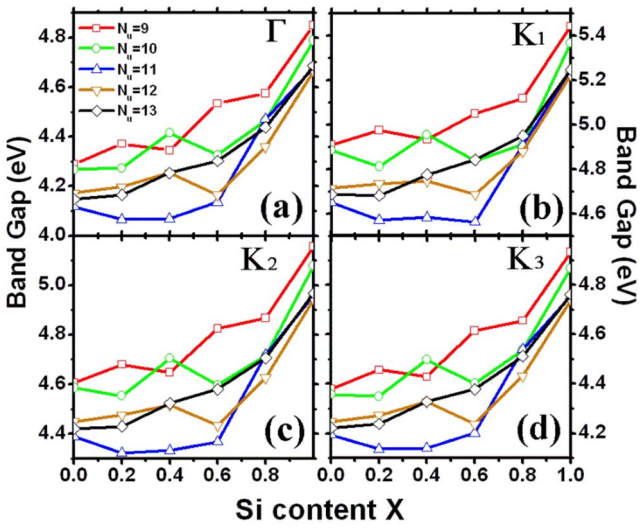

FIG. 13. (Color online) Band gap evolution for the different k points used in the calculation (a)–(d), (see Table I), as a function of the radial dimension of the tubes. At the Γ(0,0,0) point (a), the band gaps have their minimum values, increasing as the content of silicon. The same behavior with the silicon content is observed at the other k points.

bands associated to different functional groups; in particular, the bands due to the H-O-H bending of water and to the structural groups O-H are located near 3500 and 1630 cm^{-1}, respectively.[50] The broadband centered at around 1000 cm^{-1} has contributions attributed to the stretching of Si-O and Si-O-Al.[51,52] The position of the Si-O stretch band depends on the Al/Si ratio, shifting the maximum to higher wave numbers for a lower Al/Si ratio.[53] Finally, the peak at 560 cm^{-1} has been ascribed to the O-Si-O bending vibration.

Theoretically, the vibrational spectra can be obtained by two approaches; in the first approach parametrized force fields are used to get these spectra with the advantage of the fastness of the calculation, but the validation of the force fields for specific systems should be argued. The force field methodology has been employed by Tamura *et al.*[11] for the calculation of vibrational modes and strain energies of imogolite fibers using a parametrized three-body interaction potential for models with periodic boundary conditions and cell dimensions of $7.20\times7.20\times5.04$ nm^3, where the Fourier transform of the velocity autocorrelation function of the atoms was used. The imogolite spectrum obtained with this force field shows a good agreement with the Si-O vibrations near 1000 cm^{-1}, whereas the Al-O vibrations were not identified and the O-H stretching was observed at higher wave numbers. Recently, Konduri *et al.*[12] analyzed the strain energy and the vibrational properties in models of isolated imogolite tubes, from $N_u=18$ to 48, using the CLAYFF force field. The frequencies of the imogolite models were obtained from a parametrized Lagrangian that depends on the Al-O and Si-O interatomic distances and on the number of aluminum atoms in the tube, finding a good agreement for the Al-O-Al frequencies (583 cm^{-1}) and for the Al-O-Si frequencies (1091 cm^{-1}).

In the second approach, the interatomic forces are obtained from *ab initio* calculations with the advantage, at least theoretically, of a better description of the interatomic forces; however, these kinds of calculations are computationally expensive for systems with hundreds of atoms as is the case of Imo-Si cells. Therefore in order to obtain a first notion of the frequency spectra this was calculated, to optimize computational resources, for the Γ point of the most likely natural imogolite, Imo-Si-$N_u=10$. The *ab initio* calculation of the normal modes were carried out on the geometry optimized structure using the same DFT parameters employed for the geometry optimization. Figure 14(a) shows the total spectrum of frequencies obtained from the DFT calculation, where the intensity of each frequency was computed as the summation of the corresponding norms of the eigenvectors associated to each atom in the Hessian matrix. The comparison between the experimental IR spectra reported by Tamura *et al.*[11] and Johnson *et al.*[50] and our theoretical DFT calculation shows that there are common peaks in the region from 3200 to 3800 cm^{-1} and in the region from 1400 to 1200 cm^{-1}. There is an empty frequency region from 1200 to 3200 cm^{-1}. Experimentally, the peak at 1630 cm^{-1} is attributed to the presence of water in the samples; this fact explains why this peak does not appear in our theoretical spectra.

In order to distinguish the different atomic contributions to the frequency spectrum, the atomic partial contribution in each frequency was obtained and the partial intensity frequencies (PFI) were determined; this spectrum shows two main regions, see Fig. 14(b). In the first region, from ~0 to 1000 cm^{-1} the frequency spectrum has contributions from all the atoms in the imogolite structure, where the contributions from the different atomic radial layers to the frequency spectrum are shown. The layer notation used in Fig. 14(b) is the same as that of Fig. 12. The common movement of atoms in the ~0 to 1000 cm^{-1} region allows one to classify these vibrations as phonons. In the second region, from 3200 to 3800 cm^{-1}, the presence of localized atomic contributions is observed coming mainly from O-H vibrations of the inner O_2-H_1 layers, 3200 to 3400 cm^{-1}, and outer O_6-H_7 layers, from 3700 to 3800 cm^{-1}, therefore these modes can be classified as localized modes. The correlation among the frequencies of different atomic pairs in the imogolite structure was analyzed by defining the pair frequency correlation (PFC) between the atoms x and atoms y as "$PFC_{x,y}=(PFI)_x\times(PFI)_y$," where the $(PFI)_x$ denotes the partial intensity frequencies associated to the atom x in the radial direction of the imogolite arrangement. The various $PFC_{x,y}$ associated to the nearest neighbors in the radial direction are shown in Fig. 15. The O-H correlations come from the $PFC_{H_1\text{-}O_2}$ showing peaks in the regions from 3200 to 3400 cm^{-1} and from 1000 to 1200 cm^{-1}. On the other hand the $PFC_{H_7\text{-}O_6}$ shows peaks from 800 to 1000 cm^{-1} and a narrow peak distribution between 3700 and 3800 cm^{-1} that corresponds to the characteristic O-H oscillations where oxygen is three-fold coordinated, as in kaolinite and outer imogolite O-H arrangements,[54] see Fig. 15. The Si-O oscillations are associated to the $PFC_{Si_3\text{-}O_2}$ and the $PFC_{Si_3\text{-}O_4}$ showing in both cases peaks in the region between 800 and 1200 cm^{-1} centered at ~1000 cm^{-1}, as reported in the literature, see

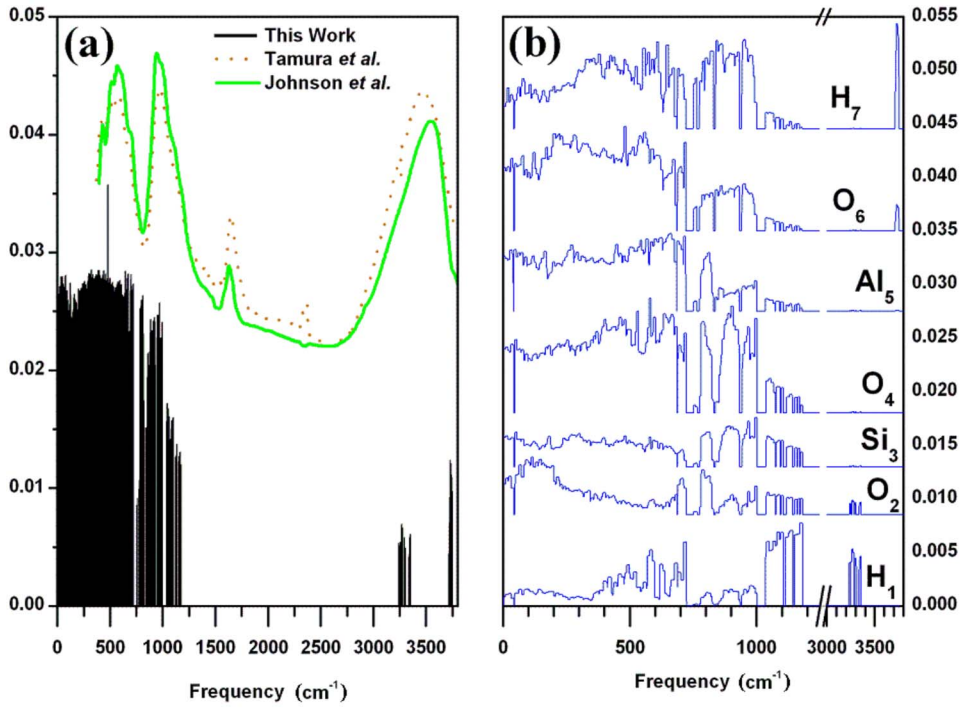

FIG. 14. (Color online) (a) Calculated total intensity frequencies (TIF) of Imo-Si $N_u=10$ compared to the experimental results reported by Tamura *et al.* (Ref. 11) and Johnson *et al.* (Ref. 50). The vibrations in the region from 0 to 1200 cm^{-1} are phononic modes associated to collective movements of all the atoms in the fiber. The region between 3100 and 3800 cm^{-1} shows localized modes associated to O-H vibrations. (b) Partial Intensity Frequencies (PIF) of Imo-Si $N_u=10$.

Fig. 15. Finally, the Al-O normal modes show intensities weaker than the Si-O normal modes, as can be seen by comparing the PFCs of Si-O with $PFC_{Al_5\text{-}O_4}$ and $PFC_{Al_5\text{-}O_5}$ in Fig. 15; nevertheless, the presence of oscillations in the region from 800 to 1000 cm^{-1} can be associated to the characteristic Al-O vibrations reported in the literature.

V. CONCLUSIONS

In this theoretical work we have calculated, from first principles, the structural and electronic properties of imogolite-like structures as a function of silicon content [$X=Si/(Si+Ge)$] and as a function of the number of gibbsite cell units, N_u, for models with periodic boundary conditions along the axial direction. A cylindrical unit cell length of 8.4 to 8.5 Å is experimentally reported in the literature for the imogolite structure, close to the experimental values for the gibbsite structure. In this work the imogolite tubular structure was calculated using DFT at three different levels of approximation: DN basis set and Γ point in the reciprocal space (DN-Γ), DN basis set and various k points (Table I) (DN-k), and DNP basis set and various k points (Table I) (DNP-k), finding the minimum position of the cylindrical cell length at 8.80 Å for the DN-Γ approximation, 8.72 Å for DN-k, and 8.62 Å when the DNP-k description was used. The difference among the calculated values and the experimental results may be due to a possible dependence of the axial length of the unit cell with curvature. In order to discern if this is the case, a sequence of quantum geometry optimizations for the flat imogolite structure, which corresponds to a tube of infinite radius, was carried out finding that for DNP-k the minimum configuration leads to cell lengths $a=4.9$ Å and $b=8.46$ Å. The b cell length corresponds to the cylindrical cell length in the imogolite, and the calculated value is within the experimentally reported interval. This result suggests a possible radius dependence of the cell length or the necessity of a more precise calculation in the k points description.

The electronic analysis in all the theoretical approaches produces similar results for the Hirshfeld charge and band gaps with values in the interval 4.75–4.94 eV for the tubular structures and 5.57 eV for the flat (infinite radius) configuration. Therefore due to this similarity in the charges and gaps, a sequence of simulations in tubular imogolites as a function of the Si/(Ge+Si) content were carried out considering as a good approximation the value of 8.72 Å for the cylindrical cell length produced by the DN-k basis.

The x-ray diffraction pattern (XRDP) of individual isolated imogolite tubes was simulated as a function of N_u and X finding that the XRDP is scarcely affected by the silicon content X and mainly affected by N_u; this phenomena was observed with both x-ray sources, $K\alpha$-Cu and Fe. The x-ray pattern shows a shifting of the two main peaks in the low 2θ region such that the larger the number N_u the lower the positions of the two main peaks. This shifting follows a linear relation whose parameters are shown in Table III. In the mesoscale level, the XRDP of bundles of imogolites was simulated finding a good agreement between the experimental x-ray structure reported by Mukherjee *et al.*[13] and a structure of 5×5 tubes formed with individual tubes with $N_u=12$, a tube-tube distance separation of 24.8 Å, and an angle between the straight lines joining the tube centers of 64°; this is practically a hexagonal configuration.

Imogolite-like structures show small changes in the atomic Hirshfeld charge analysis when N_u and X are varied. The effect of substitution of silicon by germanium represents a marginal increment of positive charge in their atomic positions that produces an increment of electronic softness of

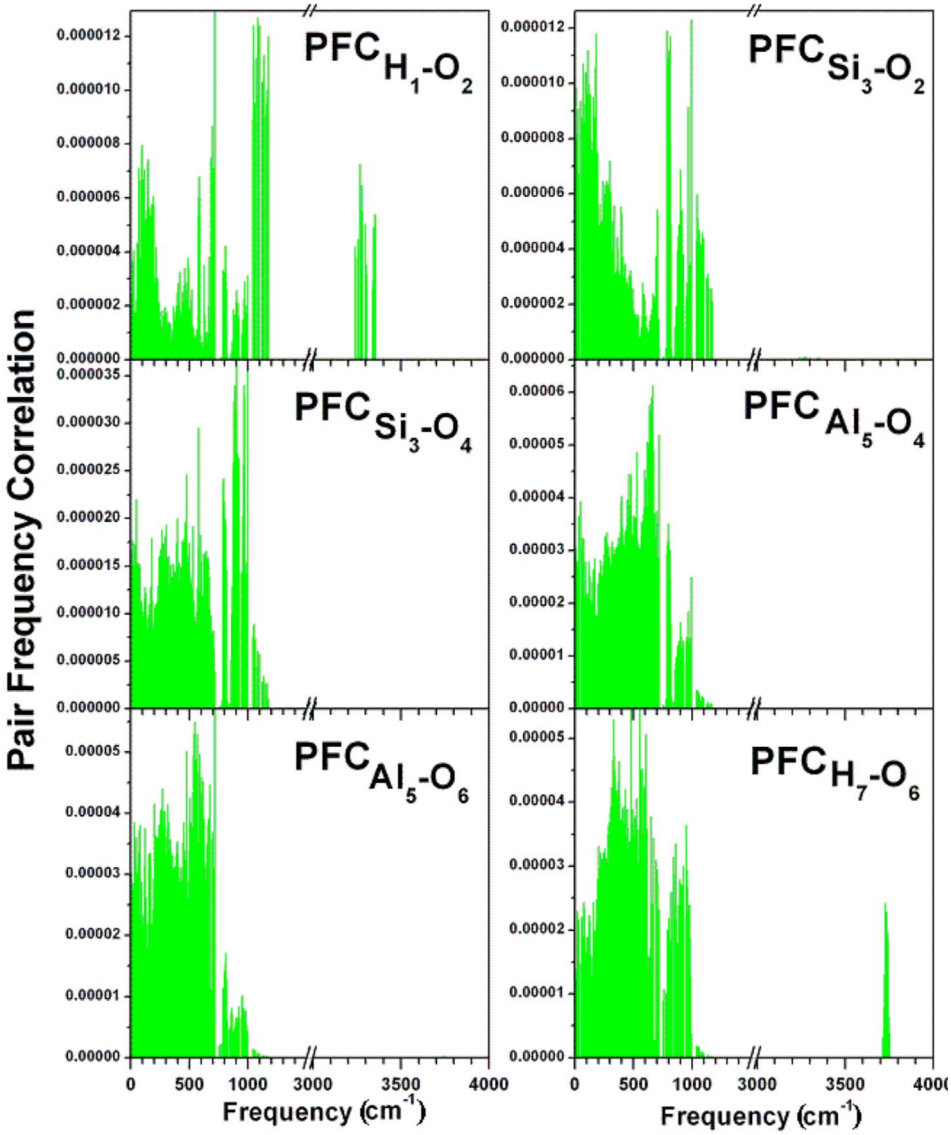

FIG. 15. (Color online) Pair frequency correlations of the nearest-neighbors radial atoms in the imogolite structure. The frequencies larger than 3000 cm^{-1} are completely due to O-H oscillations and the group of oscillations at ~1000 cm^{-1} have different PFC contributions, but are mainly due to the Si_3-O_4 oscillations layers in the imogolite structure.

the tube. The adsorption properties of cations and anions by imogolites is attributed to an external positive surface imogolite charge and an internal negative pore charge, produced by the curvature of the gibbsite layer.[47] However, in our calculations the Hirshfeld charge analysis and the potential electrostatic distribution leads to an external positive surface charge as Gustafsson *et al.*[47] proposed, but the internal charge is also positive, unlike the proposal given in Ref. 47, due to the presence of hydrogen on those surfaces in the perfect imogolite-like structures. Nevertheless, our charge results must be restricted to the ideal nonhydrated imogolites systems and then must be considered just a first approximation to the real hydrated problem, where the surface electronic structure will change substantially with *p*H and hydration.

The correlation between the electronic states and the radial position, see Fig. 12, shows that the reactive sites are in the neighborhood of HOMO energy and come from the oxygens in the various imogolite layers, but are due mainly to the internal oxygen label as O_4 in Imo-Si and Imo-Ge. The conduction band for the case of Imo-Si has its main contribution from states coming from the external hydrogen H_7, Fig. 12(a); however, for the case of Imo-Ge the conduction band has also a contribution due to the Ge_3 layer. The band gap values show an increasing behavior as a function of the silicon content in all the *k* points studied in this work, see Fig. 13. Finally, the frequency analysis shows two main regions, one characterized by collective modes (phonos) and another with only localized modes due to the O-H vibrations, qualitatively in agreement with the ir results.

ACKNOWLEDGMENTS

The author thank Ariel A. Valladares and Yosadara Ruiz-Morales for fruitful discussions. This work was supported by the Instituto Mexicano del Petróleo under Project No. D.00237.

*falvarez@imp.mx

[1] N. Yoshinaga, Soil Sci. Plant. Nutr. (Tokyo) **14**, 238 (1968).
[2] K. Wada and N. Yoshinaga, Am. Mineral. **54**, 50 (1969).
[3] V. Farmer and J. Russell, in *Soil Colloids and Their Associations in Aggregates*, edited by M. E. De Roodt *et al.* (Plenum, New York, 1973).
[4] D. Dubroeucq, D. Geissert, and P. Quantin, Geoderma **86**, 99 (1998).
[5] L. Mossin, M. Mortensen, and P. Nrnberg, Geoderma **109**, 103 (2002).
[6] V. C. Farmer, A. R. Fraser, and J. M. Tait, J. Chem. Soc., Chem. Commun. **13**, 462 (1977).
[7] S.-I Wada, A. Eto, and K. J. Wada, J. Soil Sci. **30**, 347 (1979).
[8] S.-I. Wada and C. Sakimura, Clay Sci. **30**, 347 (1979).
[9] S. Wada and K. Wada, Clays Clay Miner. **30**, 123 (1982).
[10] N. Yoshinaga and S. Aomine, Soil Sci. Plant. Nutr. (Tokyo) **8**, 22 (1962).
[11] K. Tamura and K. Kawamura, J. Phys. Chem. B **106**, 271 (2002)
[12] S. Konduri, S. Mukherjee, and S. Nair, Phys. Rev. B **74**, 033401 (2006).
[13] S. Mukherjee, V. M. Bartlow, and S. Nair, Chem. Mater. **17**, 4900 (2005).
[14] C. P. G. Cradwick, V. C. Farmer, J. D. Russell, C. R. Masson, K. Wada, and N. Yoshinaga, Nature (London) **240**, 187 (1972).
[15] L. A. Bursill, J. L. Peng, and L. N. Bourgeois, Philos. Mag. A **80**, 105 (2000).
[16] K. Kajiwara, N. Donkai, Y. Fujiyoshi, Y. Hiraki, H. Urakawa, and H. Inagaki, Bull. Inst. Chem. Res., Kyoto Univ. **63**, 320 (1985).
[17] W. C. Ackerman, D. M. Smith, J. C. Huling, Y.-W. Kim, J. K. Bailey, and C. J. Brinker, Langmuir **9**, 1051 (1993).
[18] K. Kajiwara, N. Donkai, Y. Fujiyoshi, and H. Inagaki, Makromol. Chem. **187**, 2895 (1986).
[19] J. D. Russel, W. J. McHardy, and A. R. Fraser, Clay Miner. **8**, 87 (1969).
[20] V. Farmer and A. Fraser, in *International Clay Conference 1978* (Elsevier Science, Amsterdam, 1979).
[21] K. Wada, in *Minerals in Soil Environments*, 2nd ed. (Soil Science Society of America, Madison, WI, 1989).
[22] L. Denaix, I. Lamy, and J. Y. Bottero, Colloids Surf., A **158**, 315 (1999).
[23] Y. Hirohisa, J. Michalik, J. Sadlo, J. Perlinska, S. Takenouchi, S. Shimomura, and Y. Uchida, Appl. Clay Sci. **19**, 173 (2001).
[24] M. A. Wilson, G. S. H. Lee, and R. C. Taylor, Clays Clay Miner. **50**, 48 (2002).
[25] J. Karube and Y. Abe, Clays Clay Miner. **46**, 322 (1998).
[26] S. Imamura, Y. Hayashi, K. Kajiwara, H. Hocino, and C. Taito, Ind. Eng. Chem. Res. **32**, 600 (1993).
[27] F. Ohashi, S. Tomura, K. Akaku, S. Hayashi, and S. I. Wada, J. Mater. Sci. **39**, 1799 (2004).
[28] S. Imamura, T. Kokubu, T. Yamashita, Y. Okamoto, K. Kajiwara, and H. Kanai, J. Catal. **160**, 137 (1996).
[29] L. L. Marzán and A. Philipse, Colloids Surf., A **90**, 95 (1994).
[30] G. H. Koenderink, S. G. J. M. Kluijtmans, and A. P. Philipse, J. Colloid Interface Sci. **216**, 429 (1999).
[31] J. Hu, K. Kannangara, M. A. Wilson, and N. Reddy, J. Non-Cryst. Solids **347**, 224 (2004).
[32] Z. Abidin, N. Matsue, and T. Henmi, J. Comput.-Aided Mater. Des. **14**, 5 (2007).
[33] B. J. Delley, J. Chem. Phys. **92**, 508 (1990).
[34] B. J. Delley, J. Chem. Phys. **113**, 7756 (2000).
[35] S. D. I., DMol3, User Guide, release 4.0.
[36] J. P. Perdew and Y. Wang, Phys. Rev. B **45**, 13244 (1992).
[37] F. Ohashi, S. Tomura, K. Akaku, S. Hayashi, and S.-I Wada, J. Mater. Sci. **39**, 1799 (2004).
[38] M. Tani, C. Liu, and P. M. Huang, Geoderma **118**, 209 (2004).
[39] S. D. C. Diffraction, Module of Cerius2 by ACCELRYS Corp.: San Diego, CA, 2001
[40] P. I. Pohl, J.-L. Faulon, and D. M. Smith, Langmuir **12**, 4463 (1996).
[41] A. McCutcheon, J. Hu, G. S. Kamali Kannangara, M. A. Wilson, and R. Narsimha, J. Non-Cryst. Solids **351**, 1967 (2005).
[42] M. A. Wilson, G. S. H. Lee, and R. C. Taylor, J. Non-Cryst. Solids **296**, 172 (2001).
[43] S. J. van der Gaast, K. Wada, S.-I. Wada, and Y. Kakuto, Clays Clay Miner. **33**, 237 (1985).
[44] H. Hoshino, H. Urakawa, N. Donkai, and K. Kajiwara, Polym. Bull. **36**, 257 (1996).
[45] C. Clark and M. McBride, Clays Clay Miner. **32**, 291 (1984).
[46] J. B. Harsh, S. J. Traina, J. Boyle, and Y. Yang, Clays Clay Miner. **40**, 700 (1992).
[47] J. Gustafsson, Clays Clay Miner. **49**, 73 (2001).
[48] K. Egashira and S. Aome, Clay Sci. **4**, 2331 (1974).
[49] M. D. Segall, P. J. D. Lindan, M. J. Probert, C. J. Pickard, P. J. Hasnip, S. J. Clark, and M. C. Payne, J. Phys.: Condens. Matter **14**, 2717 (2002).
[50] L. M. Jonhson and T. J.Pinnavaia, Langmuir **6**, 307 (1990).
[51] J. J. Fitzgerald, C. Murali, C. O. Nebo, and M. C. Fuerstenau, J. Colloid Interface Sci. **151**, 299 (1992).
[52] V. C. Farmer, M. J. A. R. Adams, A. R. Fraser, and F. Palmieri, Clay Miner. **18**, 459 (1983).
[53] T. Henmi, K. Tange, T. Minagawa, and N. Yoshinaga, Clays Clay Miner. **29**, 124 (1981).
[54] H. Marel and P. Krohmer, Contrib. Mineral. Petrol. **22**, 73 (1969).